The method of fundamental solution for water wave-structure interaction

Z. Razafizana[1, 3], R. Adolphe[2], R. Rabevala[1]

[1]Department of Mechanics, Polytechnic School of Antsiranana, Madagascar

[2]Department of Physics, Antananarivo University, Madagascar

[3]School of Civil Engineering and Naval Technology, Higher Institute of Technology, Antsiranana, Madagascar

Corresponding: razafizana.zatianina@gmail.com

Abstract

This paper presents the method of fundamental solution for water wave-structure interaction analysis with multiple cylinders. The method of fundamental solution (MFS) is strong-form of boundary meshless collocation method. Its numerical solution is approximated by a linear combination of fundamental solutions in terms of sources, which are placed on the fictitious boundary outside the domain of the problem to avoid the singularities of fundamental solutions at origin. In this study, two types of ocean engineering structures, circular and elliptical cylinders are considered. Numerical results show the efficiency and accuracy of the method in comparison with the singular boundary method (SBM). The near trapped mode phenomenon of four and sixteen hard cylinder structures are revisited.

Keywords: Method of fundamental solutions, strong form, meshless boundary method, collocation method, water wave-structure interaction

1. Introduction

Water wave-structure interaction is one of important topic and has been attracted the intention of engineers in ocean engineering communities [1-4]. It is a phenomenon which occurs in a system where a water wave causes the structure to deform, in turn, changes the boundary condition of water fluid system. The interactions of multiple-cylinder-array structure may result in hydrodynamic loads and wave run up on the individual-cylinder structure that differ significantly from the loads and run up they would experience in isolation [5-12]. And it can cause significant damage to offshore structures. Therefore, numerical simulation of these two water wave-structure interaction problems is essential to provide some reference on effective design for safe and economic offshore structures. Accurate computation of this phenomenon has impact on offshore production and the economics of countries.

Several numerical methods have been proposed to solve the water wave-structure interaction problems [6-8]. However their numerical method require the construction of a tedious and difficult mesh and are computationally costly and mathematically troublesome. To overcome these difficulties, investigators proposed new numerical methods, which called boundary meshless collocation methods [9-15].

In this paper, we propose the method of fundamental solution (MFS), which is a well-known strong-form boundary meshless collocation method. The method requires fictitious boundary to eliminate the numerical integral of the singular fundamental solutions in the boundary element method (BEM) [16-18]. The MFS is available for different type of problems including elliptic, time-dependent parabolic, free boundary, and coefficient and boundary inverse problems [19-21]. The method is practicable and easy to implement in complex geometry problems. The method has also advantages of high convergence rate.

In this study, two types of ocean engineering structure, circular and elliptical cylinders, are considered. The governing equation and the method of fundamental solution (MFS) for water wave-structure are introduced in the second section. The third section presents the accuracy, efficiency of the MFS in comparison with the analytical solution and the near-trapped mode phenomena for multiple cylinders. The fourth section concludes this article with some remarks.

2. Water wave-structure interaction analysis

2.1. Governing equation

Assuming that the ocean water is incompressible, non-viscous and irrotational fluid. The governing equation of water wave-structure interaction is given by

$$\nabla^2\Phi\left(x_1,x_2,x_3,t\right)=0, \qquad \left(x_1,x_2,x_3,t\right)\in\Omega \tag{1}$$

where ∇, Ω and Φ are the Laplace operator, the domain of interest and the velocity potential, respectively. The boundary conditions are

- Bottom boundary condition:

$$\frac{\partial\Phi}{\partial n}=0, \qquad x_3=-H\left(x_1,x_2\right)\in\Omega \tag{2}$$

- Kinematic free-surface boundary condition:

$$\frac{\partial\alpha}{\partial t}+\frac{\partial\Phi}{\partial x_1}\frac{\partial\alpha}{\partial x_1}+\frac{\partial\Phi}{\partial x_2}\frac{\partial\alpha}{\partial x_2}=\frac{\partial\Phi}{\partial x_3}, \qquad x_3=\alpha\left(x_1,x_2\right)\in\Omega \tag{3}$$

- Dynamic free-surface boundary condition:

$$\frac{\partial\Phi}{\partial t}+\frac{1}{2}\left\{\left(\nabla\Phi\right)^2\right\}+g\alpha=0, \quad x_3=\alpha\left(x_1,x_2\right)\in\Omega \tag{4}$$

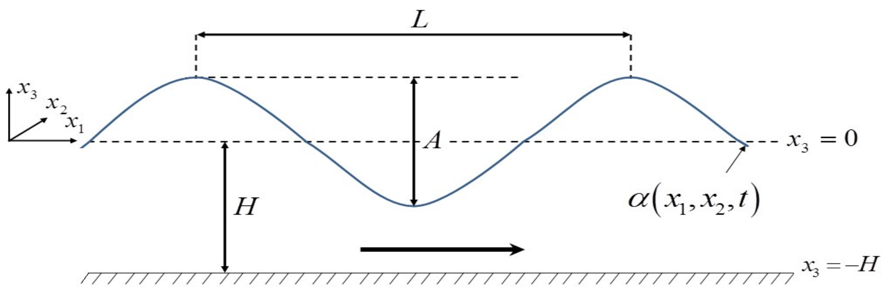

Fig.1. Spatial representation of surface elevation $\alpha(x_1, x_2, t)$

By using the method of separation of variables, we set

$$\Phi(x_1, x_2, x_3) = \Re e\{u(x_1, x_2) f(x_3)\} \tag{5}$$

where $f(x_3) = -igA/\omega \cosh(kH) / \cosh[k(x_3 + H)]$, and wavenumber k is the real root of the dispersion relationship $\omega^2 = gk\tanh(kH)$, in which g, A, ω and H are the acceleration due to the gravity, the amplitude of incident wave, the angular frequency and the water depth, respectively.

Substituting Eq. (5) into Eq. (1) - (4) and by removing the depth dependence, 3D water wave problems as shown in Fig.1 can be reduced to 2D water wave problem shown in Fig.2

$$(\nabla^2 + k^2) u(x_1, x_2) = 0, \qquad (x_1, x_2) \in \Omega \tag{6}$$

$$u(x) = \overline{u}, \qquad x \in \Gamma_D \tag{7}$$

$$q(x) = \frac{\partial u(x)}{\partial n} = \overline{q}, \qquad x \in \Gamma_N \tag{8}$$

$$\lim_{r_j \to \infty} r_j^{1/2} (\partial/\partial r_j - ik) u(x) = 0 \tag{9}$$

where u, D, N, r_j and n are the potential field, unbounded region in $\Re^2$, the Euclidean distance and the unit outward normal vector, respectively. And $i = \sqrt{-1}$, $\overline{u}$, $\overline{q}$ are known functions, Eq. (9) is the famous Sommerfeld radiation condition at infinity.

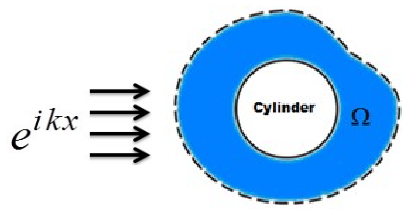

Fig. 2. Sketch of 2D water wave problems

2.2. The method of fundamental solution (MFS)

The approximate solution in the MFS is given by

$$\begin{cases} u(x_m) = \sum_{j=1}^{N} \varepsilon_j G(x_m, s_j), & x_m \in \Omega \setminus \Gamma_D \\ q(x_m) = \dfrac{\partial u(x_m)}{\partial n} = \sum_{j=1}^{N} \varepsilon_j \dfrac{\partial G(x_m, s_j)}{\partial n}, & x_m \in \Omega \setminus \Gamma_N \end{cases} \tag{10}$$

where ε_j, Ω, Γ_D and Γ_N represent the j^{th} unknown coefficients to be determined, the unbounded domain, the essential boundary (Dirichlet) and natural boundary (Neumann) conditions, respectively. The function $G(x_m, s_j)$ is a fundamental solution given by $G(x_m, s_j) = \frac{i}{4} H_0^{(1)}\left(kr_{mj}(x_m, s_j)\right)$ for exterior problems in 2D. In which $i = \sqrt{-1}$, Euclidean distance $r_{mj} = \|x_m - s_j\|_2$ and $H_0^{(1)}$, x_m, s_j denote the Hankel function of the first kind of order zero, the m^{th} collocation points on the physical boundary and the j^{th} source points which lie outside Ω, respectively.

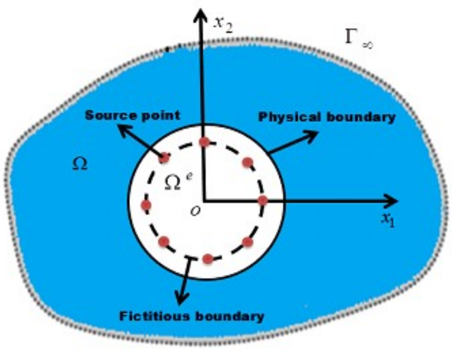

Fig. 3. Sketch and node distribution of the MFS for exterior problems

- The mathematical model for multiple cylinder problems:

$$\begin{cases} \left(\nabla^2 + k^2\right) u^p\left(x_1, x_2\right) = 0, & \left(x_1, x_2\right) \in \Omega_1, \quad p = 1, 2, \dots n \\ q = \dfrac{\partial u^p\left(x_1, x_2\right)}{\partial n} = 0, & \left(x_1, x_2\right) \in \Gamma_\infty, \quad p = 1, 2, \dots n \\ \lim\limits_{x \to \infty} r^{\frac{1}{2}} \left[\dfrac{\partial\left(u - u_i\right)}{\partial r} - ik\left(u - u_i\right) \right] = 0, & \left(x_1, x_2\right) \in \Gamma_\infty \end{cases} , \tag{11}$$

Where $u = u_i + u_s$, in which u_i, u_s are the incident wave and scattered wave, respectively.

- The fundamental solutions (MFS) for multiple cylinders is represented as

$$\begin{cases} u_2^p\left(x_m\right) = u_i\left(x_m\right) + \sum\limits_{j=1}^{N^{(p)}} \overline{\varepsilon}_j^{(p)} \overline{G}\left(x_m, s_j^{(p)}\right), & x_m \in \Omega_1 \setminus \Gamma_D \\ q_2^p\left(x_m\right) = \dfrac{\partial u_i\left(x_m\right)}{\partial n} + \sum\limits_{j=1}^{N^{(p)}} \overline{\varepsilon}_j^{(p)} \dfrac{\partial \overline{G}\left(x_m, s_j^{(p)}\right)}{\partial n}, & x_m \in \Omega_1 \setminus \Gamma_N, \\ \lim\limits_{r_j \to \infty} r_j^{1/2} \left(\partial/\partial r_j - ik\right)\left(u_2 - u_i\right) = 0, & x_m \in \Gamma_\infty \end{cases} \tag{12}$$

where p represent the number of cylinder ($N = \sum_{p=1}^{n} N^{(p)}$) and the fundamental solution $G\left(x_m, s_j\right) = \overline{G}\left(x_m, s_j\right) = \frac{i}{4} H_0^{(1)}\left(kr_{mj}\left(x_m, s_j\right)\right)$ for exterior problems in 2D, Euclidean distance $r_{mj} = \left\|x_m - s_j\right\|_2$ and ε_j, n_x and N represent the j^{th} unknown coefficient to be determined by the imposing the boundary condition, and the outward normal unit on the collocation points x_m and the number of source points s_j, respectively.

For the multiple cylinders the unknown coefficients and the source points are represented as

$$\begin{cases} \overline{\varepsilon_j} = \left[\left\{ \overline{\varepsilon}_1^{(1)} \right\}, \left\{ \overline{\varepsilon}_2^{(2)} \right\}, \dots\dots\dots, \left\{ \overline{\varepsilon}_N^{(n)} \right\} \right] \\ s_j = \left[s_1^{(1)}, \dots . s_{N^{(1)}}^{(n)}, \dots . s_1^{(n)} \dots .., s_{N^{(n)}}^{(n)} \right] \end{cases} \tag{13}$$

3. Numerical results

The efficiency, accuracy, and convergence of the MFS are tested by calculating the root mean square error (*RMSE*), the relative and error (*Rerr*), which are respectively defined as

$$RMSE(u) = \sqrt{\frac{1}{NT}\sum_{i=1}^{NT}\left|u(i)-\bar{u}(i)\right|^2} \tag{14}$$

$$Rerr(u) = \sqrt{\frac{1}{NT}\sum_{i=1}^{NT}\left|\frac{u(i)-\bar{u}(i)}{\bar{u}(i)}\right|} \tag{15}$$

where u and $\bar{u}$ are the numerical and the exact solutions of the total potential field. NT is the number of tested points in the domain, which are uniform angular distributed on the boundary.

3.1 Example 1: Water wave-structure interaction with one circular cylinder

We consider a plan wave $u_i = e^{ik(x_1\cos\theta_{inc}+x_2\sin\theta_{inc})}$ scattered by rigid vertical cylinder (Neumann type). The total field of scattering is $u = u_i + u_s$ which satisfies the Helmholtz equation in 2D (Eq. 6). The boundary condition on rigid cylinder is given by

$$\frac{\partial u_i(x)}{\partial n}+\frac{\partial u_s(x)}{\partial n}=0, \qquad x\in\Omega \tag{16}$$

And the analytical solution of scattering field is given by [22]

$$u_s(r,\theta) = -\frac{J_1^{(1)}(kp)}{H_1^{(1)}(kp)}H_0^{(1)}(kr) - 2\sum_{t=1}^{\infty} i^t \frac{-kpJ_{t-1}^{(1)}(kp)+tJ_t^{(1)}(kp)}{kpH_{t-1}^{(1)}(kp)-tH_{t-1}^{(1)}(kp)} H_t^{(1)}(kr)\cos(t\theta) \tag{17}$$

where $H_t^{(1)}$, $J_t^{(1)}$, (r,θ), k and p represent the t^{th} order Hankel function of the first kind, the t^{th} order Bessel function of the first kind, polar coordinates of the domain point, the wavenumber and the radii of the circular domain, respectively.

Fig. 4 represents errors analysis of the MFS for various numbers of nodes in example 1 from a rigid cylinder. We fixed the fictitious radius, the wavenumber *k=1*, incident wave $\theta_{inc}=0$ and the fictitious radius *r= 0.7*. From this figure, we can observe that the numbers of *N=100* provide better results.

Fig. 5 shows the analytical and numerical solutions from rigid cylinder with wavenumber *k=1*, fictitious radius 0. 7 incident angle $\theta_{inc}=0$. MFS and analytical solutions are in good agreement. The method rapidly converges.

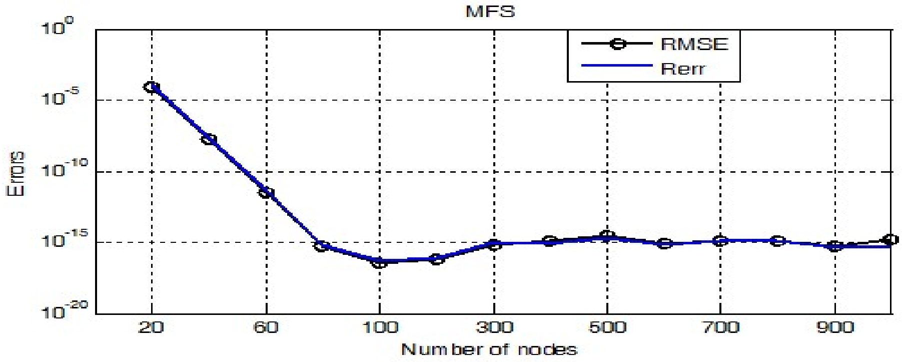

Fig. 4 Errors analysis of the MFS for various numbers of nodes with fictitious radius *r=0.7*, with wavenumber *k=1*, incident wave $\theta_{inc}=0$

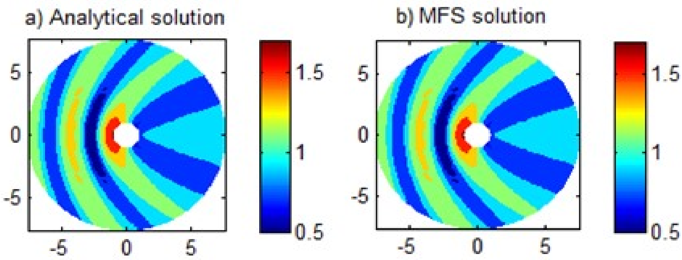

Fig. 5. Numerical and analytical solutions of rigid cylinder with *k=1*: (a) Analytical solution, (b) MFS solution with fictitious radius 0. 7 and incident angle $\theta_{inc}=0$.

3.2 Example 2: Water wave-structure interaction with multiple cylinders

a) - Water wave-structure interaction analysis with four circular and elliptical cylinders

We consider four rigid cylinders subjected to a plan wave $u_i = e^{ik(x_1\cos\theta_{inc}+x_2\sin\theta_{inc})}$ with incident angle $\theta_{inc}=0^o$. The radius of each circular cylinders is *a=0.4* separation central distance of two cylinders $b=0.5$ as shown in Fig. 6(a). The semi-major axis and semi-minor axis of elliptical cylinders are a_j = *0.4* and b_j=*0.2* (*j=1, 2, 3, 4*), respectively (Fig. 6(ii)). The separation distance between each elliptical cylinder to the origin of the system is O_jO *=0.6* (*j=1, 2, 3, 4*).

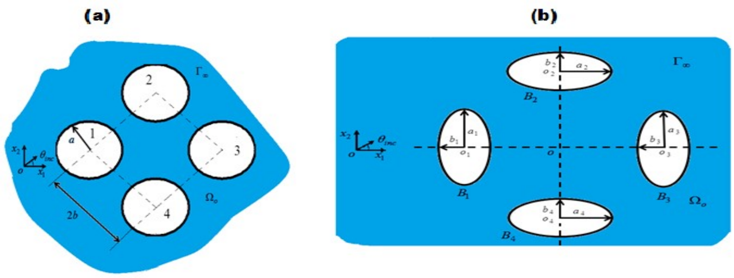

Fig. 6. Sketch of 2D water wave interactions by an array of four rigid cylinders for near-trapped mode analysis: (a) circular cylinder and (b) elliptical cylinder

Fig. 7 plots the variation of free-surface elevation in the vicinity of four rigid cylinders from the SBM (Fig.7a) and MFS (Fig.7b) with incident angles $\theta_{inc} = 0^o$ and at wavenumber *ka=4.08482* for circular cylinders (Fig.7i) and at wavenumber *ka=3.1497* for elliptical cylinders (Fig.7ii).

The near-trapped mode phenomenon is revisited [4, 10], the maximum amplitude is 160 times of amplitude of incident wave for circular cylinders (Fig.7i) and 120 for elliptical cylinders (Fig.7ii). The SBM and MFS are in good agreement.

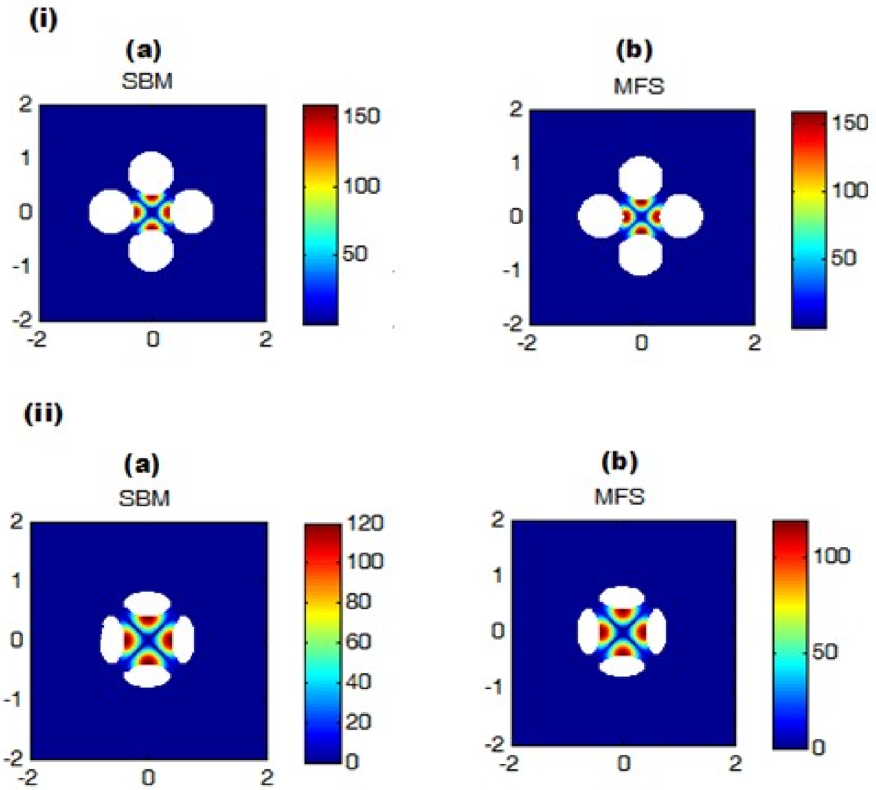

Fig. 7. The variation of free-surface elevation in the vicinity of four rigid cylinders with incident angle $\theta_{inc} = 0^o$ from (i) circular cylinders at wave number *ka=4.08482* and (ii) elliptical cylinders at *ka=3.1497*: (a) SBM solution and (b) MFS solution

b) - Water wave-structure interaction analysis with sixteen circular and elliptical cylinders

We consider a plane $u_i = e^{ik(x_1 \cos\theta_{inc} + x_2 \sin\theta_{inc})}$ scattered by an array of sixteen hard cylinders. In the simulation, we set *a=0.4*, *b=0.5*, *ka=4.08482*, *H=2* and $\theta_{inc} = 0$ for circular cylinders and *a=0.4*, *b=0.2*, *ka=3.1497*, *H=2*, d=0.6 and $\theta_{inc} = 0$ for elliptical cylinders.

Fig. 8a displays the free-surface elevation in the vicinity of sixteen rigid circular cylinders with wavenumber *ka=4.08482*, incident angle $\theta_{inc} = 0$ and number of node *N= 100* of each cylinder. The near-trapped mode phenomenon [4, 10] is revisited, the maximum amplitude of runup is 120 times. We can observe from this figure that the distribution of the wave amplitude inner sides of the cylinders is not the same. The coming wave impinging the array cylinders oscillates and has its maximum (crest) and minimum (through). Here, the wave elevation is maximum inner sides of the four cylinders at the top and bottom and it is minimum inner sides of array of cylinders at the middle.

Fig. 8b shows the free-surface elevation in the vicinity of sixteen rigid elliptical cylinders with wavenumber *ka=3.1497*, incident angle $\theta_{inc} = 0$ and number of node *N= 300*. The maximum value appears on the inner sides of the cylinders is over 70 times of incident wave amplitude. Here, the wave elevation is minimum inner sides of the third, eighth, ninth and fourteenth cylinders and it is maximum inner sides of others cylinders.

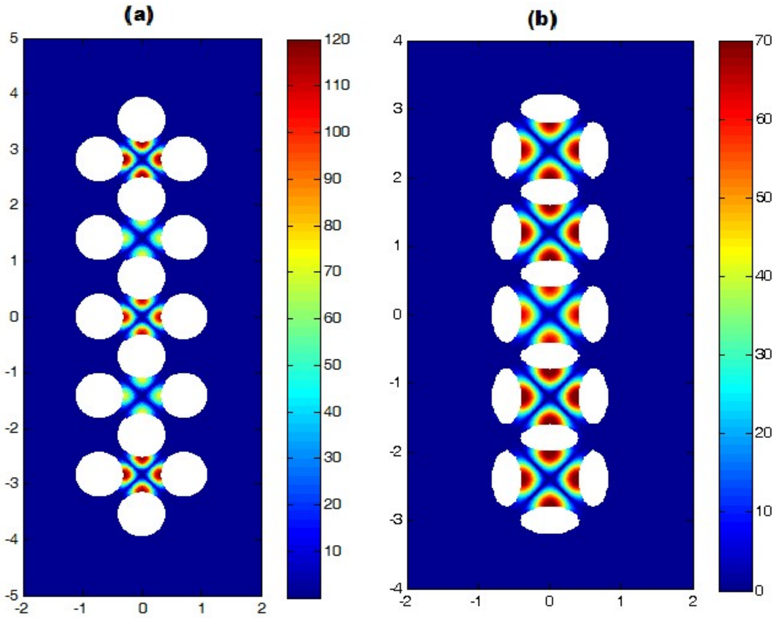

Fig. 9. The free-surface elevation in the vicinity of sixteen hard cylinders with incident angle $\theta_{inc} = 0$ and number of node *N= 100* of each cylinder: (a) circular cylinders, wavenumber *ka=4.08482*, (b) elliptical cylinders, wavenumber *ka=3.1497*

c) – Numerical Investigation

In this section, we study the near-trapped mode in the case of irregular arrangement of ten and sixteen cylinders with incident angle $\theta_{inc} = 0$. The displacement of each cylinder center apart from its original periodical position is defined as follows

$$\begin{cases} \Delta x_j = \gamma_j (b-a)\tau \cos(2\pi\gamma_j) \\ \Delta y_j = \gamma_j (b-a)\tau \sin(2\pi\gamma_j) \end{cases}, \quad (18)$$

where γ_j, τ and a represent a random variable in the range of [0, 1], a global disorder parameter and the radii of cylinders, respectively. Here we set $\gamma_j = 1$ and $\tau = 1$. Fig. 10 shows the disorder displacement in the irregular arrangement for sixteen cylinders. This figure is applicable to an array of the circular and elliptic cylinders.

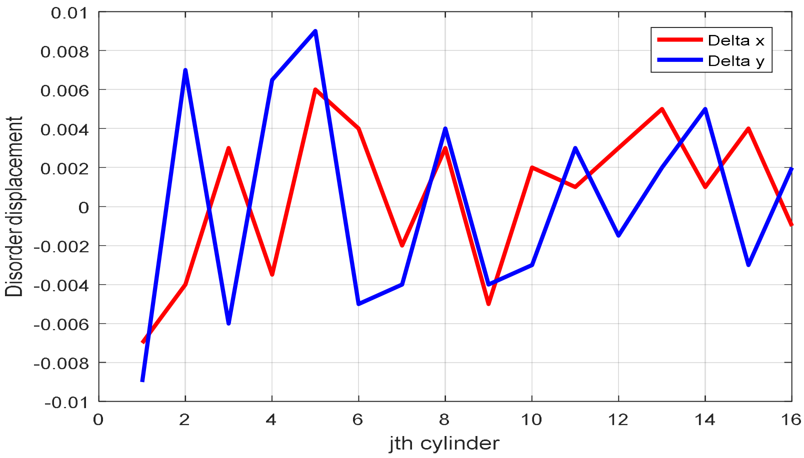

Fig. 10. Disorder displacement in the irregular arrangement for sixteen cylinders

Fig. 11a plots free-surface elevation in the vicinity of sixteen hard circular cylinders with wavenumber *ka=4.08482*, incident angle. The results show that the disorder treatment can weaken the free-surface elevation on inner sides of the cylinders. The maximum amplitude is 5 times of incident wave.

Fig. 11b represents the free-surface elevation in the vicinity of sixteen hard elliptical cylinders for with wavenumber *ka=3.1497* incident angle $\theta_{inc} = 0$. For this case, the maximum amplitude is 4.5 times of incident wave.

4. Conclusions

We have applied the MFS to the problem of water wave-structure interactions with multiple cylinders. Two types of cylinders, circular and elliptical cylinder structures, are considered. The present method is accurate, efficient and stable. The near-trapped mode phenomena was examined. The maximum amplitude on inner sides of elliptical cylinders is much lower than the one on inner sides of circular cylinders. It is found that the disorder treatment can suppress the occurrence of the near-trapped phenomena. After comparing with the results obtained in the literature, good agreements were observed.

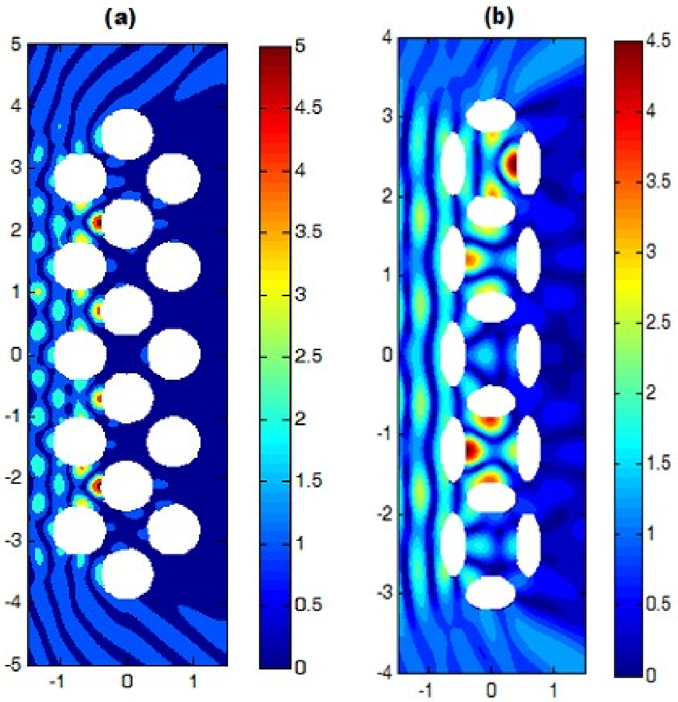

Fig. 11. The free-surface elevation in the vicinity of sixteen hard cylinders with incident angle $\theta_{inc} = 0$ and number of node *N= 100*: (a) Circular cylinders, *ka=4.08482*, (b) elliptical cylinders, *ka=3.1497*

References

[1] Chen, J. T. Null-field integral equation approach for boundary value problems with circular boundaries [J]. Proceeding of ICCES 2005, 2005, 407-412.

[2] Chen, J.T., Lee, Y.T. Interaction of water waves with array of cylinders using Null-field integral equations [C]. The 14th National Computational Fluid Dynamics Conference: CFD14 A-023. Conference Proceedings, 2007.

[3] Chen, J.T., Lee, Y.T., Lin, Y.J. Interaction of water waves with vertical cylinders using null-field integral equations [J]. Applied Ocean Research, 2009, 31 (2): 101-110.

[4] Chen, J.T., Lin, Y.J., Lee, Y.T., Wu, C.F. Water wave interaction with surface-piercing porous cylinders using the null-field integral equations [J]. Ocean Engineering, 2011a, 38 (2-3): 409-418.
[5] Chen, J.T., Wu, C.F., Chen, I.L., Lee, J.W. On near-trapped modes and fictitious frequencies for water wave problems containing an array of circular cylinders using a null-field boundary integral equations [J]. European Journal of Mechanics - B/Fluids, 2012, 32: 32-44.
[6] Evans, D. V., Porter, R. Near-trapping of waves by circular arrays of vertical cylinders [J]. Applied Ocean Research, 1997a, 19: 83-99.
[7] Chen, J.T., Lee, J.W. A semi-analytical method for near-trapped mode and fictitious frequencies of multiple scattering by an array of elliptical cylinders in water waves [J]. Physics of Fluids, 2013, 25 (9): 79-103.
[8] Chen, J.T., Wu, C.F., Lee, J.W., Hsiao, Y.C. Analysis of water wave problems containing single and multiple cylinders by using the degenerate kernel method [J]. ISOPE Journal, 2011b, 21 (1): 13-21.
[9] Fu, Z.J., Chen, W. Water wave interaction with multiple surface-piercing porous cylinders by singular boundary method [C]. 11th International Conference of Numerical Analysis and Applied Mathematics 2013: ICNAAM 2013. AIP Conference Proceedings, 2013, 928-931.
[10] Zatianina, R., Fu, Z.J. Singular boundary method for water wave problems [J]. Ocean Engineering, 2015, 96: 330-337.
[11] Fu, Z. J., Chen. W., Wen, P., H., Zhang, C. Z. Singular boundary method for wave propagation analysis in periodic structures [J]. Journal of Sound and Vibration, 2018, 425: 170-188.
[12] Li, J., P., Fu, Z., J., Chen, W. Numerical investigation on the obliquely incident water wave passing through the submerged breakwater by singular boundary method [J]. Computers & Mathematics with Applications, Jan 2016, 71: 381-390.
[13] Tang, Z., C., Fu, Z., J., Zheng, D., J., Huang, J., D. Singular boundary method to simulate scattering of SH wave by the canyon topography [J]. Advances in Applied Mathematics and Mechanics, 2018, 10(4): 912-924.
[14] Qu, W., Z., Chen, W., Fu, Z., J., Gu, Y. Fast multipole singular boundary method for Stokes flow problems [J]. Mathematics & Computers in Simulation, 2018, 146: 57-69.
[15] Li, J., P., Chen, W., Fu, Z., J. Numerical Investigation on Convergence Rate of Singular Boundary Method [J]. Mathematical Problems in Engineering, 2016, 13: 3564632.
[16] Alexander, H.D.C., Cheng, D.T. Heritage and early history of the boundary element method [J]. Engineering Analysis with Boundary Elements, 2005, 29: 268–302.
[17] Golberg, M.A., Chen C.S. The theory of radial basis functions applied to the BEM for inhomogeneous partial differential equations [J]. Boundary Elements Communications, 1994, 5: 57–61.
[18] Brebbia, C.A. Boundary Element Methods [C]. Proc. of the 8th Int. Conf. on BEM, Como 1986, Springer-Verlag, 1986, Berlin.
[19] Wang, H., Qin, Q. Some problems with the method of fundamental solution using radial basis functions [J]. Acta Mechanica Solida Sinica, 2007, 20 (1).
[20] Balakrishman, K., Ramachandran, P.A. The method of fundamental solutions for linear diffusion-reaction equations [J]. Math. Comput. Model., 2000, 31(1-3): 221-237.
[21] Li, J., P., Qin, Q., H., Fu, Z., J. A dual-level method of fundamental solutions for three-dimensional exterior high frequency acoustic problems [J]. Applied Mathematical Modelling, 2018, 63: 558-576.
[22] Liu, H., Zou, J. Zeros of the Bessel and spherical functions and their applications for uniqueness in inverse acoustic obstacle scattering [J]. IMA Journal of Applied Mathematics, 2007, 72: 817-831.